Electron propagator theory calculations of molecular photoionization cross sections: The first-row hydrides

G. M. Seabra
Department of Chemistry, Kansas State University, 111 Willard Hall, Manhattan, Kansas 66506-3701

I. G. Kaplan
Instituto de Investigaciones en Materiales, Universidad Nacional Autónoma de México, Apartado Postal 70-360, México, D.F., 04510, México

V. G. Zakrzewski and J. V. Ortiz[a)]
Department of Chemistry, Kansas State University, 111 Willard Hall, Manhattan, Kansas 66506-3701

(Received 22 April 2004; accepted 24 May 2004)

Together with ionization potentials, cross sections provide valuable information for the interpretation of photoelectron spectra. We have developed a program to perform *ab initio* calculations of photoionization cross sections within the electric dipole approximation using electron propagator theory. Applications to the first-row hydrides CH_4, NH_3, H_2O, and HF, using several approximations for the propagator self-energy and the plane-wave and orthogonalized-plane-wave approximations to represent the photoelectron, as well as comparison to experimental data, are presented. This program is implemented within the quantum chemistry package GAUSSIAN. © *2004 American Institute of Physics.* [DOI: 10.1063/1.1773135]

I. INTRODUCTION

Photoelectron spectroscopy is a powerful tool for probing the electronic structure of atoms and molecules and is used in a wide variety of areas ranging from atmospheric and space to biomedical and biophysical sciences.[1–3] Electron binding energies and corresponding intensities provide diverse insights into chemical bonding. The variation of photoionization intensities with the energy of the incoming radiation and the character of both the initial and final states provide ample opportunities for probing electronic structure.

From a chemist's perspective, it is valuable to discern patterns of chemical bonding and reactivity from spectroscopic experiments, especially if they can be mapped onto familiar one-electron concepts. Hartree-Fock molecular orbital theory provides such an interpretation, where Koopmans's theorem[4] enables the use of orbital energies as estimates of the ionization energies and electron affinities. This picture has been used for qualitative interpretation of photoelectron spectra. However, at this level of theory the effects of orbital relaxation in the final state and electron correlation, which are often required for the correct assignment of the spectra, are ignored.

To improve quantitative agreement with experiment, generalization of wave functions and energy functionals to include those effects, such as configuration interaction and many-body perturbation theory, can be applied.[5] However, accompanying this improvement in energy comparisons there is often a complex structure of many-electron wave functions and energies that sacrifices the one-electron picture, thus obscuring the qualitative interpretation of the spectra.

Electron propagator theory (EPT) provides an alternative approach for this problem.[6–19] This formalism can, in principle, provide exact electron binding energies that include final-state orbital relaxation as well as electron correlation effects. To each electron binding energy calculated in this way, there is an associated one-electron function that is rigorously related to the many-electron wave functions of the initial and final states. This association enables the interpretation of spectra in terms of one-electron concepts, without necessarily compromising the quality of quantitative results.

Routine, accurate calculations of ionization energies are already feasible using propagator theory in the most recent versions of quantum chemical software packages such as GAUSSIAN.[20] Unfortunately, the situation is not quite the same with the corresponding cross sections. Although a considerable quantity of theoretical work has been devoted to the calculation of photoionization cross sections,[21–34] commonly used quantum mechanical packages available today still lack this ability.

We have developed a program, implemented as part of the quantum chemistry package GAUSSIAN,[20] to perform *ab initio* calculations of photoionization cross sections using EPT, within the electric dipole approximation. Applications to a test set of molecules composed of the first-row hydrides CH_4, NH_3, H_2O, and HF are presented, using different EPT approximations and the plane-wave[21] and orthogonalized-plane-wave[25] approximations to represent the photoelectron.

II. THEORY

A. Electron propagator theory

The physical significance of the propagator lies in its poles, i.e., the energies E where singularities lie, which cor-

a)Electronic mail: ortiz@ksu.edu

respond to ionization energies, $E_n(N-1)-E_0(N)$ and electron affinities, $E_0(N)+E_m(N+1)$. In spectral form, the r, s element of the electron propagator matrix is

$$G_{rs}(E)\equiv\langle\langle a_r^\dagger;a_s\rangle\rangle = \lim_{\eta\to 0}\left[\sum_n \frac{\langle\Psi_0^N|a_r^\dagger|\Psi_n^{N-1}\rangle\langle\Psi_n^{N-1}|a_s|\Psi_0^N\rangle}{E+E_n(N-1)-E_0(N)-i\eta} + \sum_m \frac{\langle\Psi_0^N|a_s|\Psi_m^{N+1}\rangle\langle\Psi_m^{N+1}|a_r^\dagger|\Psi_0^N\rangle}{E-E_m(N+1)+E_0(N)+i\eta}\right], \quad (1)$$

where the indices r and s are general, orthonormal spin-orbitals, $|\Psi_0^N\rangle$ is the N-electron reference state, $a_r^\dagger$ and a_s are field operators that change the number of electrons by one, and the limit is taken with respect to η because of the integration required in a Fourier transform from the time-dependent representation of the propagator. Associated to each pole is a residue (the numerator of the term responsible for the singularity) which can be written in terms of the Feynman-Dyson amplitudes (FDAs),

$$U_{i,n}^{\mathrm{IE}}=\langle\Psi_n^{N-1}|a_i|\Psi_0^N\rangle \quad (2)$$

and

$$U_{b,m}^{\mathrm{EA}}=\langle\Psi_m^{N+1}|a_b^\dagger|\Psi_0^N\rangle. \quad (3)$$

The superscripts indicate whether the respective pole pertains to an ionization energy (IE) or an electron affinity (EA). The FDAs can be used to build the Dyson Orbitals (DO) that, in the case of IEs, are expressed as

$$|g_n\rangle=\sum_{i=1}^N |\phi_i\rangle U_{i,n}^{\mathrm{IE}}=\sum_{i=1}^N |\phi_i\rangle\langle\Psi_n^{N-1}|a_i|\Psi_0^N\rangle=\sum_{i=1}^N b_{in}\phi_i. \quad (4)$$

These orbitals may be considered to be overlaps between the initial N-electron state and the final $(N-1)$-electron state. The integral is over the coordinates of all electrons except one (x_1), yielding a one-electron function that can be written as a linear combination of HF canonical molecular orbitals (ϕ_i). It can also be shown that finding the poles of the propagator is equivalent to solving a pseudoeigenvalue problem that reads[13]

$$[F+\Sigma(E)]|g_n\rangle=\epsilon_n|g_n\rangle, \quad (5)$$

where the Fock operator F is supplemented by the energy-dependent, nonlocal self-energy operator, $\Sigma(E)$, which includes relaxation and correlation effects. The eigenvalues of this equation are the electron binding energies (IEs and EAs), while the eigenfunctions are the respective DOs.

The propagator matrix can be defined in a more convenient way by the use of a superoperator metric defined by[6]

$$(\mu|\nu)=\langle\Psi_0^N|[\mu^\dagger,\nu]_+|\Psi_0^N\rangle, \quad (6)$$

where μ and ν are field operators that change the number of electrons by one (X) and by the introduction of the identity $(\hat{I})$ and Hamiltonian $(\hat{H})$ superoperators, defined by the relations

$$\hat{I}X=X \quad (7)$$

and

$$\hat{H}X=[X,\hat{H}]_-. \quad (8)$$

The r, s element of the electron propagator can thus be written as

$$\langle\langle a_r^\dagger;a_s\rangle\rangle\equiv G_{rs}(E)=(a_r|(E\hat{I}-\hat{H})^{-1}a_s), \quad (9)$$

which, in matrix notation, reads

$$\mathbf{G}(E)=(\mathbf{a}|(E\hat{I}-\hat{H})^{-1}\mathbf{a}). \quad (10)$$

After defining $\mathbf{u}$ to be the vector of all X field operators and partitioning it into the primary operator space $\mathbf{a}$ (with hole h and particle p subspaces) and an orthonormal secondary operator space $\mathbf{f}$ (with products of two annihilators and one creator of the $2ph$ and $2hp$ types), the propagator matrix can be written as

$$\mathbf{G}(E)=[1\ \ 0]\begin{bmatrix} E1-(\mathbf{a}|\hat{H}\mathbf{a}) & -(\mathbf{a}|\hat{H}\mathbf{f}) \\ -(\mathbf{f}|\hat{H}\mathbf{a}) & E1-(\mathbf{f}|\hat{H}\mathbf{f})\end{bmatrix}^{-1}\begin{bmatrix}1\\0\end{bmatrix}. \quad (11)$$

Poles of the propagator will occur at values of E that are equal to the eigenvalues ω_n of the superoperator Hamiltonian matrix

$$\omega_n\begin{bmatrix}\mathbf{U}_{a,n}\\ \mathbf{U}_{f,n}\end{bmatrix}=\begin{bmatrix}(\mathbf{a}|\hat{H}\mathbf{a}) & (\mathbf{a}|\hat{H}\mathbf{f})\\ (\mathbf{f}|\hat{H}\mathbf{a}) & (\mathbf{f}|\hat{H}\mathbf{f})\end{bmatrix}\begin{bmatrix}\mathbf{U}_{a,n}\\ \mathbf{U}_{f,n}\end{bmatrix} \quad (12)$$

or

$$\mathbf{U}\omega=\hat{\mathbf{H}}\mathbf{U}. \quad (13)$$

The eigenvectors of the superoperator Hamiltonian matrix are normalized in the space containing the h, p, $2ph$, and $2hp$ operators such that

$$\sum_i^{occ}|U_i|^2+\sum_a^{virt}|U_a|^2+\sum_{i<j}^{occ}\sum_a^{virt}|U_{ija}|^2 + \sum_{a<b}^{virt}\sum_i^{occ}|U_{iab}|^2=1. \quad (14)$$

In this formulation, the Dyson orbital can be written as

$$|g_n\rangle=\sum_i^{occ}U_i|\phi_i\rangle+\sum_a^{virt}U_a|\phi_a\rangle. \quad (15)$$

The sum of the squared coefficients of the DO defines the pole strength. Pole strengths above 0.9 indicate that the Koopmans one-electron description is qualitatively valid. Diagonal approximations (see below) should provide accurate representations of the ionization process if there is a single, dominant term in Eq. (15). Lower pole strengths (below 0.8) are generally an indication that shake-up states are to be expected, and nondiagonal approximations are recommended to accurately describe the ionization.

After a few elementary matrix manipulations, the inverse propagator matrix can be expressed as

$$\mathbf{G}^{-1}(E)=E1-(\mathbf{a}|\hat{H}\mathbf{a})-(\mathbf{a}|\hat{H}\mathbf{f})[E1-(\mathbf{f}|\hat{H}\mathbf{f})]^{-1}(\mathbf{f}|\hat{H}\mathbf{a}). \quad (16)$$

Writing the zeroth order inverse propagator as

$$\mathbf{G}_0^{-1}(E)=E1-(\mathbf{a}|\hat{H}_0\mathbf{a}), \quad (17)$$

and the self-energy matrix as

$$\Sigma(E)=(\mathbf{a}|\hat{V}\mathbf{a})+(\mathbf{a}|\hat{H}\mathbf{f})[E1-(\mathbf{f}|\hat{H}\mathbf{f})]^{-1}(\mathbf{f}|\hat{H}\mathbf{a}), \quad (18)$$

one may write the Dyson equation as

$$\mathbf{G}^{-1}(E)=\mathbf{G}_0^{-1}(E)-\Sigma(E). \quad (19)$$

The inverse in the self-energy matrix expression of Eq. (18) is calculated through an infinite expansion by the recursion formula

$$(\mathbf{A}-\mathbf{B})^{-1}=\mathbf{A}^{-1}+\mathbf{A}^{-1}\mathbf{B}(\mathbf{A}-\mathbf{B})^{-1}. \quad (20)$$

Because $(\mathbf{f}|\hat{H}\mathbf{f})$ includes nondiagonal terms in first order or higher, terms of all orders in the self-energy matrix can be generated.

Each of the blocks of the superoperator Hamiltonian matrix may be evaluated to various orders, and several approximate propagators are defined in terms of this matrix. Poles to second order are obtained by the choice

$$\hat{\mathbf{H}}^{(\text{Second Order})}=\begin{bmatrix}(\mathbf{a}|\hat{H}\mathbf{a})^{(0)} & (\mathbf{a}|\hat{H}\mathbf{f})^{(1)}\\ (\mathbf{f}|\hat{H}\mathbf{a})^{(1)} & (\mathbf{f}|\hat{H}\mathbf{f})^{(0)}\end{bmatrix}. \quad (21)$$

The $2p$-h TDA (two-particle, one-hole Tamm-Dancoff approximation) approximation is complete only through second order. The secondary states are now treated consistently through first order, providing access to inner-valence states where contributions from shake-up configurations are important. Here the approximate superoperator Hamiltonian matrix reads

$$\hat{\mathbf{H}}^{(2p\text{-}h\ \text{TDA})}=\begin{bmatrix}(\mathbf{a}|\hat{H}\mathbf{a})^{(0)} & (\mathbf{a}|\hat{H}\mathbf{f})^{(1)}\\ (\mathbf{f}|\hat{H}\mathbf{a})^{(1)} & (\mathbf{f}|\hat{H}\mathbf{f})^{(1)}\end{bmatrix}. \quad (22)$$

To improve the treatment of the main (valence) states, the $2p$-h TDA can be extended by a self-consistent treatment of the $(\mathbf{a}|\hat{H}\mathbf{a})$ block, resulting in an infinite partial summation for the self-energy that is complete through third order, and by inclusion of second-order terms in the couplings between the primary and secondary ionization operators. This is the basis for the extended $2p$-h TDA or third-order algebraic diagrammatic construction, or ADC(3), methods.[8]

In the so-called *quasiparticle* methods, off-diagonal elements in the self-energy matrix are explicitly neglected. This approximation is justified on the basis that experimental results on the valence ionization energies (and also electron affinities) indicate that the contribution from these elements is small, often having a negligible effect on the binding energies and DOs. As a result, the DOs will be proportional to the original (HF canonical) molecular orbitals (MOs), the electrons being subject to an effective potential described by the self-energy matrix. The eigenvalues of Eq. (5) can be calculated iteratively by

$$E=\epsilon_p+\Sigma_{pp}(E), \quad (23)$$

where ϵ_p is the canonical MO energy. In many applications, the self-energy matrix is expanded through third order and the usual initial guess, $E\approx\epsilon_p+\Sigma_{pp}(\epsilon_p)$, is equal to the energy difference between the initial and final states obtained using second- or third-order perturbation theory with frozen (initial state) orbitals, when second- or third-order expansions for Σ_{pp} are used, respectively. Because second-order results typically overestimate the correlation corrections while third-order results underestimate them, three scaling procedures known as outer valence green's function (OVGF) methods *A*, *B*, and *C* have been developed to improve accuracy,[9] as well as numerical criteria to choose from the three methods.[10]

A somewhat different derivation of the electron propagator approximations employs an asymmetric metric inspired by the coupled-cluster parametrization of the reference state. Numerical tests on the importance of various terms generated in this manner leads to the partial third-order approximation, P3.[11] This method has been reviewed recently[15] and has been successfully applied to a variety of molecules.[16–19] The P3 method has proven to be more accurate than OVGF methods in many applications and is computationally more efficient, since it does not require the evaluation of electron repulsion integrals with four virtual indices. It corresponds to the following choice of the superoperator Hamiltonian matrix,

$$\hat{\mathbf{H}}^{(\text{P3})}=\begin{bmatrix}\hat{\mathbf{H}}^{(0)}_{h,h} & \hat{\mathbf{H}}^{(0)}_{h,p} & \hat{\mathbf{H}}^{(1)}_{h,2hp} & \hat{\mathbf{H}}^{(1)}_{h,2ph}\\ \hat{\mathbf{H}}^{(0)}_{p,h} & \hat{\mathbf{H}}^{(0)}_{p,p} & \hat{\mathbf{H}}^{(1)}_{p,2hp} & \hat{\mathbf{H}}^{(1)}_{p,2ph}\\ \hat{\mathbf{H}}^{(2)}_{2hp,h} & \hat{\mathbf{H}}^{(2)}_{2hp,p} & \hat{\mathbf{H}}^{(1)}_{2hp,2hp} & \hat{\mathbf{H}}^{(0)}_{2hp,2ph}\\ \hat{\mathbf{H}}^{(1)}_{2ph,h} & \hat{\mathbf{H}}^{(1)}_{2ph,p} & \hat{\mathbf{H}}^{(0)}_{2ph,2hp} & \hat{\mathbf{H}}^{(0)}_{2ph,2ph}\end{bmatrix}, \quad (24)$$

while keeping the resulting self-energy terms through third order, making the quasiparticle (diagonal) approximation and omitting $(\mathbf{a}|\hat{V}\mathbf{a})$ terms from Eq. (18). The NR2[14] method (nondiagonal, renormalized second-order extension to the P3 method) consists of solving for the eigenvalues of the matrix in Eq. (24) but with the $2hp,p$ block expanded only through first order, and omitting the $(\mathbf{a}|\hat{V}\mathbf{a})$ terms as well. The neglect of second-order terms in the $2hp,p$ block is justified by numerical tests that show these terms to have a negligible effect on IE poles.

B. The photoionization process

The first calculations of the photoionization cross section of molecules were performed by Kaplan and Markin[22,23] and by Lohr and Robins[24,25] (see also Refs. 26–28). In these studies, the photoionization cross section was calculated in the first order of time-dependent perturbation theory. The initial molecular state and the ion were described in the Hartree-Fock approximation, while the ejected electron was described by a plane wave[22–24] or orthogonalized plane wave.[25,27,28] In contrast to the former approach, the employment later on of DOs for the determination of photoionization cross sections[7,29–34] allowed description of electron correlation effects while preserving, at the same time, all benefits of the one-electron description.

In first-order time-dependent perturbation theory, the probability of transition per unit time (transition rate, w) is given by Fermi's Golden Rule:[35]

$$w(\mathbf{k}_e)=\frac{2\pi}{\hbar}\sum_n |\langle\Psi_0^N|\mathbf{B}|\Psi_{n\mathbf{k}_e}^N\rangle|^2\rho_{\mathbf{k}_e}(E), \quad (25)$$

where $\rho_{\mathbf{k}_e}(E)$ is the density of states for the photoelectron with the wave vector $\mathbf{k}_e$; $\mathbf{B}$ is the many-electron perturbation Hamiltonian for the interaction between radiation and matter; Ψ_0^N is the initial state wave function, which is an eigenfunction of the time-independent Hamiltonian operator H_N; and $\Psi_{n\mathbf{k}_e}^N$ is the antisymmetrized wave function for the final state n, where one electron has been excited to the continuum orbital $\phi_{\mathbf{k}_e}$ with energy $\epsilon_K=\hbar\omega-\mathrm{IP}=|\hbar\mathbf{k}_e|^2/2m_e$. The final state wave function is represented as

$$|\Psi_{\mathbf{k}}^N\rangle=\frac{1}{\sqrt{2}}(a_{\mathbf{k}\alpha}^+|\Psi_\beta^{N-1}\rangle-a_{\mathbf{k}\beta}^+|\Psi_\alpha^{N-1}\rangle)$$
$$=\sqrt{2}(a_{\mathbf{k}\alpha}^+|\Psi_\beta^{N-1}\rangle), \tag{26}$$

where we used the spin-raising operator S_+ such that $S_+|\Psi_\beta\rangle=|\Psi_\alpha\rangle$, and which follows the commutation rule $[S_+,a_{\mathbf{k}\beta}^+]=a_{\mathbf{k}\alpha}^+$.

The many-electron perturbation Hamiltonian $\mathbf{B}$ can be written from its one-electron counterpart as

$$\mathbf{B}=\sum_{ij} V_{ij}E_{ij}, \tag{27}$$

where E_{ij} is the unitary group generator $E_{ij}=a_{i\alpha}^+a_{j\alpha}+a_{i\beta}^+a_{i\beta}$ that follows the commutation rule

$$[E_{ij},a_{\mathbf{k}\alpha}^+]=\delta_{j\mathbf{k}}a_{i\alpha}^+. \tag{28}$$

The interaction of a photon of wave vector $\mathbf{k}_p$ with the ith electron is given by

$$\hat{V}=\frac{-e}{m_ec}\mathbf{A}_i\cdot\mathbf{p}_i, \tag{29}$$

$$\mathbf{A}_i=A_0\mathbf{n}e^{i(\mathbf{k}_p\cdot\mathbf{r}_i)}, \tag{30}$$

$$\mathbf{p}_i=-i\hbar\vec{\nabla}_i. \tag{31}$$

Inserting Eqs. (26)–(28) into Eq. (25) yields an expression in terms of the DO, g_n,[29]

$$w(\mathbf{k}_e)=\frac{2\pi}{\hbar}|\langle g_n|\hat{V}|\phi_{\mathbf{k}_e}\rangle|^2\rho_{\mathbf{k}_e}(E). \tag{32}$$

To obtain the differential cross section, it is useful to notice that the energy transported per unit time (rate of energy transport) and per unit area by an electromagnetic wave of frequency ν is given by the magnitude of the Poynting vector, $S=\omega^2A_0^2/2\pi c$. If the Poynting vector is multiplied by the differential cross section $d\sigma$, the *energy transport rate* results. This rate must be the same as obtained by the product of the transition rate ω by the photon energy $\hbar\omega$. Equating these two results, the differential cross section for photoionization can be written as

$$d\sigma=\frac{(2\pi)^2c}{\omega A_0^2}|\langle g_n|\hat{V}|\phi_{\mathbf{k}_e}\rangle|^2\rho_{\mathbf{k}_e}(E). \tag{33}$$

The density of states for the free electron in the solid angle $d\Omega$ is[36]

$$\rho_{\mathbf{k}_e}(E)=\left(\frac{L}{2\pi}\right)^3\frac{m_ek_e}{\hbar^2}d\Omega. \tag{34}$$

Therefore, for the differential cross section of photoionization, one obtains the following expression:

$$\frac{d\sigma}{d\Omega}=\left(\frac{m_e}{\hbar^2}\right)\frac{L^3k_ec}{2\pi\omega A_0^2}|\langle g_n|\hat{V}|\phi_{\mathbf{k}_e}\rangle|^2. \tag{35}$$

If the wavelength of the incident photon can be considered as large compared to the molecular dimensions, the exponential in Eq. (30) may be approximated as unity. This is the basis for the electric dipole approximation.

C. The wave function for the ejected electron

The simplest representation for the continuum orbital is a plane wave (PW) with the wave vector $\mathbf{k}_e$.[21] Taking it to be normalized inside the volume of a large cubic box of edge L (Refs. 23–25) the free electron wave function will be

$$\phi_{\mathbf{k}_e}\rightarrow\varphi_{\mathbf{k}_e}=\frac{1}{\sqrt{L^3}}\eta_{\mathbf{k}_e}(\mathbf{r}), \tag{36}$$

$$\eta_{\mathbf{k}_e}(\mathbf{r})=e^{i(\mathbf{k}_e\cdot\mathbf{r})}. \tag{37}$$

The plane-wave approximation ignores the influence of the positively charged molecular ion on the wave function of the ejected electron, which renders it is invalid in the vicinity of the threshold of ionization. It is a reasonable approximation in the limit of high electron kinetic energy. On the other hand, the plane-wave approximation is not able to reproduce correct angular distributions for electrons with angular momentum $l\neq0$.[21] This limitation can be partially corrected by the use of plane waves that have been Schmidt orthogonalized to the occupied bound MOs of the system.[27–33] The continuum orbital can than be represented as an orthogonalized plane wave:[25]

$$|\phi_{\mathbf{k}_e}\rangle=N\left[|\varphi_{\mathbf{k}_e}\rangle-\sum_i|\phi_i\rangle\langle\phi_i|\varphi_{\mathbf{k}_e}\rangle\right]. \tag{38}$$

As the size of the box to which the plane wave is normalized gets large, the normalization constant

$$N=\left[1-\left(\frac{L}{2\pi}\right)^{-3}\sum_i|\langle\phi_i|\eta_{\mathbf{k}_e}\rangle|^2\right]^{-1/2} \tag{39}$$

can be taken as unity.

Writing $\mathbf{P}=\langle g_n|\vec{\nabla}_i|\phi_{\mathbf{k}_e}\rangle$, we have, for the orthogonalized plane wave (OPW) approximation,

$$\mathbf{P}^{\mathrm{OPW}}=\left[i\mathbf{k}_e\langle g_n|\eta_{\mathbf{k}_e}\rangle-\sum_j\langle g_n|\vec{\nabla}_i|\phi_j\rangle\langle\phi_j|\eta_{\mathbf{k}_e}\rangle\right]. \tag{40}$$

In the PW case, the second term in brackets is zero.

D. The spectrum of a gaseous sample

The random orientation of the molecules in a gaseous sample requires that all incoming photon directions be averaged by integrating over the solid angle of the incoming radiation ($d\Omega_p=\sin\theta\,d\theta\,d\phi$). In general

$$\frac{d\sigma}{d\Omega}=\left(\frac{e^2}{m_e}\right)\frac{k_e}{2\pi\omega c}\frac{\int|\mathbf{n}\cdot\mathbf{P}|^2 d\Omega_p}{\int d\Omega_p}$$

$$=\left(\frac{e^2}{m_e}\right)\frac{k_e}{2\pi\omega c}\frac{1}{4\pi}\int|\mathbf{n}\cdot\mathbf{P}|^2 d\Omega_p. \quad (41)$$

If the incident beam is unpolarized, one must also average over the incident photon polarizations

$$|\mathbf{n}\cdot\mathbf{P}|^2=\frac{1}{2}(|\mathbf{n}_1\cdot\mathbf{P}|^2+|\mathbf{n}_2\cdot\mathbf{P}|^2). \quad (42)$$

The two polarization directions are perpendicular to the photon propagation vector $\mathbf{k}_p$. These three vectors form a right-hand system of axes, and therefore

$$|\mathbf{P}|^2=|\mathbf{n}_1\cdot\mathbf{P}|^2+|\mathbf{n}_2\cdot\mathbf{P}|^2+\frac{|\mathbf{k}_p\cdot\mathbf{P}|^2}{|\mathbf{k}_p|^2}. \quad (43)$$

Now, Eq. (41) can be written as

$$\frac{d\sigma}{d\Omega}=\left(\frac{e^2}{m_e}\right)\frac{k_e}{2\pi\omega c}\frac{1}{8\pi}\int\left(|\mathbf{P}|^2-\frac{|\mathbf{k}_p\cdot\mathbf{P}|^2}{|\mathbf{k}_p|^2}\right)d\Omega_p, \quad (44)$$

$$\frac{d\sigma}{d\Omega}=\left(\frac{e^2}{m_e}\right)\frac{k_e}{2\pi\omega c}\frac{|\mathbf{P}|^2}{8\pi}\int(1-\cos^2\theta)d\Omega_p, \quad (45)$$

$$\frac{d\sigma}{d\Omega}=\left(\frac{e^2}{m_e}\right)\frac{k_e}{6\pi\omega c}|\mathbf{P}|^2. \quad (46)$$

Integration of Eq. (46) over the solid angle $d\Omega$ yields the angle-averaged photoionization cross section.

III. IMPLEMENTATION

Equation (46) was implemented in GAUSSIAN, using both PW and OPW approximations to represent the ejected electron, closely following the work of Deleuze *et al.*[33] Writing the molecular orbitals as linear combinations of atomic orbitals, the **P** vector representing the overlap between the DO and the photoelectron can be conveniently written as

$$\mathbf{P}^{\mathrm{OPW}}=\sum_{m'}b^*_{mn}\sum_p\sum_{i=1}^{N}\left[i\mathbf{k}_e-\sum_{m'p'}c_{mp}\Gamma_{pp'}c_{m'p'}\right]$$

$$\times c^*_{mp}\mathbf{S}(\mathbf{k}_e), \quad (47)$$

where

$$\mathbf{S}(\mathbf{k}_e)=\langle\omega_p|\eta_{\mathbf{k}_e}\rangle \quad (48)$$

and

$$\mathbf{\Gamma}_{pp'}=\langle\omega_p|\vec{\nabla}_t|\omega_{p'}\rangle. \quad (49)$$

In the PW case, the second term in brackets in Eq. (47) vanishes. The last integrals ($\Gamma_{pp'}$) are the dipole velocity integrals, while the $\mathbf{S}(\mathbf{k}_e)$ integrals represent an overlap between a plane wave and an atomic orbital.

Most computational chemistry programs (including GAUSSIAN) use the scheme proposed by Boys[37] of writing the atomic orbitals as linear combinations of Cartesian Gaussian primitive functions $[\gamma(\mathbf{r})]$ on each atomic center,

$$|\omega_p\rangle=\sum_q d_{pq}|\gamma_{pq}\rangle=\sum_q d_{pq}(N_{ijk}x^iy^jz^ke^{-ar^2}), \quad (50)$$

where the sum $i+j+k$ defines the angular momentum of the atomic orbital. Therefore,

$$\mathbf{S}(\mathbf{k}_e)=\sum_q d_{pq}\langle\gamma_q|e^{i(\mathbf{k}_e\cdot\mathbf{r})}\rangle=\sum_q d_{pq}[\langle e^{-i(\mathbf{k}_e\cdot\mathbf{r})}|\gamma_q\rangle]. \quad (51)$$

The integral in brackets in Eq. (51) is $(2\pi)^{-2/3}$ times the Fourier transform of the primitive Cartesian Gaussian function $\gamma(\mathbf{r})$. Formulas for those integrals have been derived earlier by Kaijser and Smith[38] in the convenient form of a recursive relation which permits one routine to calculate the Fourier transform of any given Cartesian Gaussian independently of the angular momentum of the atomic orbital. The Fourier transform reads

$$FT[\gamma(\mathbf{r})]=(2\pi)^{-3/2}\int e^{-i(\mathbf{p}\cdot\mathbf{r})}\gamma(\mathbf{r})d\mathbf{r}$$

$$=e^{-i\mathbf{k}\cdot\mathbf{A}}e^{-p^2/4\alpha}\prod_{i=1}^{3}(-i)^{k_i}K_{k_i}(z_i), \quad (52)$$

where

$$z_i=p_i/2\sqrt{\alpha}, \quad (53)$$

$$2\alpha K_{k+1}(z)=pK_k(z)-kK_{k-1}(z), \quad (54)$$

$$K_0=(2\alpha)^{-1/2}, \quad (55)$$

$$K_1(z)=p(2\alpha)^{-3/2}. \quad (56)$$

The integration of Eq. (46) to obtain the cross sections is done by a double Chebyshev polynomial integration.[39] In this method, the integrand is fit to a Chebyshev polynomial which is then easily integrated using the Clenshaw-Curtiss quadrature.[40]

IV. CALCULATIONS

Calculations of the photoionization cross sections of the first row hydrides CH_4, NH_3, H_2O, and HF are shown. The correlation consistent, polarized valence triple ζ (cc-pVTZ) basis set[41] with a full set of Cartesian functions was used in all calculations. Results from a related study of basis set effects on intensity calculations that will soon be published indicate that the cc-pVTZ basis set used here represents a good compromise between efficiency and accuracy.

Geometries were optimized at the MP2 level. The IEs and the respective DOs were calculated with $2ph$-TDA, ADC(3), and NR2 nondiagonal approximations to the self-energy, with the second order and P3 quasiparticle (diagonal) approximations and with canonical Hartree-Fock orbitals and energies. The cross sections were calculated for Mg $K\alpha$ incident radiation (1253.6 eV) with the PW or OPW approximations for the photoelectron.

Table I shows the absolute, angle averaged cross sections results for the outermost Dyson orbital of each molecule. Those lines were taken as reference for calculation of the relative intensities summarized in Tables II, III, IV, and V. (For comparison with the experimental values, each cross section is multiplied by the degeneracy of the respective or-

TABLE I. Photoionization cross section absolute values ($\times 10^{-27}$ m^2) for the orbitals taken as reference in the calculation of relative intensities. Values here do not include the degeneracy factor.

Method	Molecule	HF	Second order	P3	$2p$-h TDA	ADC(3)	NR2
PW	CH_4 ($1t_2$)	1.82	1.67	1.68	1.65	1.68	1.69
	NH_3 ($3a_1$)	20.73	18.59	19.01	19.79	19.78	19.94
	H_2O ($1b_1$)	28.21	25.04	26.02	24.05	24.91	24.81
	HF (1π)	59.94	53.66	55.91	51.80	53.64	53.15
OPW	CH_4 ($1t_2$)	2.73	2.51	2.52	2.47	2.52	2.50
	NH_3 ($3a_1$)	20.63	18.50	18.92	20.02	19.99	20.06
	H_2O ($1b_1$)	22.92	20.36	21.16	20.07	20.69	20.53
	HF (1π)	45.31	40.58	42.27	39.94	41.17	40.77

bital when calculating the relative intensities.) Figures 1–4 depict the ± 0.05 contours of the DOs that were generated with the program MOLDEN.[42] In all cases it is found that the DO is dominated by a single Hartree-Fock molecular orbital. The same labels are applied to both sets of orbitals. Tables VI, VII, and VIII show the shake-up configurations pertaining to the states with low pole strengths from the NR2 calculations. All contributions are summed for configurations where the same occupied orbitals are coupled to different virtual orbitals with same symmetry, and an "n" is used in column 5 to indicate the virtual orbitals. The number shown with the configuration description in column 5 is the sum of squares of the coefficients for each of the $2hp$ configurations combined [see Eq. (14)]. Only cases where this sum is above 0.1 are shown. In column 4 the total sum of all $2hp$ configurations is shown.

V. DISCUSSION

The results agree well with previous calculations using smaller basis sets.[29–33] In general, all calculations reproduce the experimental ordering of the photoionization intensities.[43–45] As expected from the nature of the PW and OPW approximations, quantitative agreement becomes poorer as the photoelectron energy decreases, and the intensities for the core ionizations are in most cases underestimated. The neglect of the electrostatic interactions with the molecular ion is a main source of errors in this region, and the PW approximation is known to be valid only in the high photoelectron kinetic energy limit. Although the orthogonalization correction to the plane wave can be considered to take this influence partially into account, both the PW and the OPW approximations fail to reproduce the experiment quantitatively for the core ionization. A better description of the photoelectron at energies closer to the threshold of ionization demands the inclusion of the electrostatic interaction with the molecular ion.

With respect to inner and outer valence orbitals, a reasonable agreement with experimental values is obtained in all cases. The program presented here has the ability to calculate the intensities for the (h,p) part of the shake-up states. The results show that adding the contributions from different shake-up lines is important for an accurate treatment of ionizations, especially for cases subject to intensity dispersion such as the inner valence ionizations in NH_3 and H_2O. Such improvement was predicted earlier by Deleuze, Pickup, and Delhalle,[33] but their program was not able to calculate those intensities at that time. Nondiagonal approximations can also improve the results when different final states corresponding to the same irreducible representation are present, as in H_2O. Whereas the correlation and relaxation corrections included

TABLE II. Calculated values for the ionization potentials (IP, in eV) and relative (%) photoionization intensities of the CH_4 molecule. Degeneracy factor is already taken into account.

	Koopmans			Second order			P3		
Orbital	IP (str)	σ_{PW}	σ_{OPW}	IP (str)	σ_{PW}	σ_{OPW}	IP (str)	σ_{PW}	σ_{OPW}
$1a_1$	304.9	33 450	22 085	291.6(0.80)	28 602	18 893	292.3(0.81)	28 877	19 077
$2a_1$	25.70	1114	755	23.43(0.88)	1063	721	23.33(0.86)	1034	701
$1t_2$	14.85	100	100	14.12(0.92)	100	100	14.27(0.92)	100	100
	$2ph$-TDA			ADC(3)			NR2		
$1a_1$	289.8(0.77)	27 535	18 209	293.0(0.81)	28 698	19 004	291.7(0.79)	27 623	18 496
$2a_1$	22.50(0.80)	976	663	23.35(0.82)	991	674	22.97(0.81)	973	669
$1t_2$	13.96(0.91)	100	100	14.42(0.92)	100	100	14.22(0.92)	100	100
	Expt.[a]								
$1a_1$	290.7	13 900							
$2a_1$	23.0	540							
$1t_2$	14.0	100							

[a]Reference 43.

TABLE III. Calculated values for the ionization potentials (IP, in eV) and relative (%) photoionization intensities of the NH_3 molecule. Degeneracy factor is already taken into account.

Orbital		Koopmans			Second order			P3		
		IP (str)	σ_{PW}	σ_{OPW}	IP (str)	σ_{PW}	σ_{OPW}	IP (str)	σ_{PW}	σ_{OPW}
$1a_1$		422.7	13 952	13 617	405.0(0.78)	11 902	11 620	407.6(0.82)	12 308	12 018
$2a_1$		31.02	562	584	27.69(0.81)	508	527	28.00(0.68)	414	430
$1e$		16.97	61	64	15.98(0.91)	62	65	16.43(0.93)	61	65
$3a_1$		11.67	100	100	10.24(0.90)	100	100	10.82(0.92)	100	100
		$2ph$-TDA			ADC(3)			NR2		
$1a_1$		404.1(0.77)	11 008	10 573	409.1(0.82)	11 791	11 332	406.9(0.80)	11 280	10 893
$2a_1$	(a)	37.83(0.03)	18	19	37.78(0.02)	17	18	37.80(0.02)	18	18
	(b)	34.63(0.02)	5	5	34.62(0.02)	6	6	34.62(0.02)	6	6
	(c)	29.52(0.15)	89	91	29.73(0.28)	168	172	29.61(0.21)	123	126
	(d)	26.60(0.40)	221	225	27.48(0.53)	292	298	27.05(0.57)	313	321
	(e)	26.29(0.25)	137	140	26.38(0.02)	8	8	26.37(0.04)	20	21
	$\Sigma(2a_1)$		471	480		491	501		479	491
$1e$		15.97(0.91)	57	60	16.62(0.93)	59	61	16.34(0.92)	59	61
$3a_1$		10.26(0.90)	100	100	11.03(0.92)	100	100	10.72(0.91)	100	100
		Expt.[a]								
$1a_1$		405.6	17 700							
$2a_1$		27.7	530							
$1e$		16.5	50							
$3a_1$		10.85	100							

[a]Reference 43.

in the EPT calculations prove very important in determining the correct ionization energies, intensity results obtained from different theory levels vary only slightly. None of the correlated methods is clearly superior and much more significant improvement to the results is noted when changing from PW to OPW, indicating the relevance of the orthogonalization correction to the plane wave, already pointed out by other authors.[25,28,33]

TABLE IV. Calculated values for the ionization potentials (IP, in eV) and relative (%) photoionization intensities of the H_2O molecule.

Orbital		Koopmans			Second order			P3		
		IP (str)	σ_{PW}	σ_{OPW}	IP (str)	σ_{PW}	σ_{OPW}	IP (str)	σ_{PW}	σ_{OPW}
$1a_1$		559.4	13 575	15 579	537.9 (0.77)	11 633	13 379	541.3(0.81)	12 404	14 262
$2a_1$		36.64	716	925	32.44 (0.77)	621	802	33.39(0.70)	544	703
$1b_2$		19.26	65	66	18.11 (0.91)	67	68	18.78(0.94)	66	67
$3a_1$		15.79	156	176	13.87 (0.90)	158	177	14.80(0.93)	157	176
$1b_1$		13.76	100	100	11.51 (0.89)	100	100	12.53(0.93)	100	100
		$2ph$-TDA			ADC(3)			NR2		
$1a_1$		537.8(0.79)	12 304	13 781	544.3 (0.84)	12 726	14 310	541.4(0.81)	12 327	13 922
$2a_1$	(a)	37.44(0.07)	55	69	37.48 (0.11)	80	102	37.45(0.09)	65	83
	(b)	33.77(0.02)	13	16	33.83 (0.14)	108	136	33.78(0.03)	26	33
	(c)	32.29(0.57)	456	574	33.40 (0.55)	430	543	32.85(0.63)	486	616
	(d)	30.16(0.19)	133	167	30.39 (0.07)	48	60	30.30(0.11)	77	98
	$\Sigma(2a_1)$		656	826		665	842		654	830
$1b_2$		18.24(0.92)	69	69	19.00 (0.94)	68	68	18.66(0.93)	68	69
$3a_1$		14.05(0.91)	182	205	15.08 (0.93)	174	195	14.61(0.92)	177	199
$1b_1$		11.75(0.91)	100	100	12.84 (0.93)	100	100	12.37(0.92)	100	100
		Expt.[a]								
$1a_1$		546.5	30 400							
		⋯	330		Broad band attributed to $2a_1$					
		34.8	200		Attributed to $3a_1$ shake up.					
$2a_1$		32.2	840							
$1b_2$		18.4	80							
$3a_1$		14.8	260							
$1b_1$		12.6	100							

[a]Reference 43.

TABLE V. Calculated values for the ionization potentials (IP, in eV) and relative (%) photoionization intensities of the HF molecule. Degeneracy factor is already taken into account.

Orbital		Koopmans			Second order			P3		
		IP (str)	σ_{PW}	σ_{OPW}	IP (str)	σ_{PW}	σ_{OPW}	IP (str)	σ_{PW}	σ_{OPW}
1σ		715.3	3433	3709	694.4(0.08)	···	···	···	···	···
2σ		43.40	265	375	39.11(0.34)	99	140	40.72(0.48)	136	193
3σ		20.70	52	57	18.94(0.92)	53	58	19.87(0.94)	52	57
1π		17.53	100	100	14.70(0.90)	100	100	15.97(0.94)	100	100
		2*ph*-TDA			ADC(3)			NR2		
1σ	(a)	848.7(0.03)	123	48	847.6(0.02)	68	64	848.1(0.03)	92	87
	(b)	838.8(0.01)	44	47	···	···	···	838.6(0.01)	37	36
	(c)	828.2(0.02)	64	127	827.5(0.01)	51	50	827.8(0.02)	57	56
	(d)	795.5(0.01)	48	3444	···	···	···	···	···	···
	(e)	786.6(0.01)	47	4	···	···	···	···	···	···
	(f)	775.4(0.03)	125	105	774.0(0.03)	114	116	774.7(0.03)	124	127
	(g)	691.9(0.81)	3208	242	699.1(0.86)	3284	3528	695.6(0.83)	3218	3466
2σ	(a)	43.46(0.02)	3	48	43.46(0.02)	3	4	43.45(0.02)	3	4
	(b)	40.73(0.25)	76	47	41.34(0.50)	144	200	40.97(0.36)	104	145
	(c)	37.68(0.62)	175	127	38.67(0.39)	108	150	38.20(0.53)	145	202
$\Sigma(2\sigma)$			*253*	*351*		*255*	*355*		*252*	*352*
3σ		19.19(0.93)	60	67	20.13(0.94)	57	63	19.68(0.93)	58	65
1π		15.10(0.92)	100	100	16.37(0.94)	100	100	15.76(0.93)	100	100
		Expt.[a]								
1σ		694.0	14 167							
2σ		39.65	417							
3σ		19.89	79							
1π		16.12	100							

[a]References 44 and 45.

It has been shown that in the sudden approximation, where final state relaxation and matrix elements describing any process other than the primary ionization are neglected, the resulting ''uncorrelated'' cross section implicitly includes the effect of one- and multi-electron transitions, i.e., is a sum of the cross section of the main ionization line plus the cross sections related to any shake-up/shake-off processes associated to it.[46] This effect can be noticed in the inner-valence ionization region for NH_3, H_2O and HF, where the intensities obtained using Koopmans's theorem reproduce the experimental intensities reasonably well. The sum of intensities from nondiagonal results related to the same final state approach the Koopmans's theorem intensity results as more terms are added in the self-energy expansion.

Pole strengths have been used as a first approximation to the relative cross sections. The results presented here indicate that such an approach may lead to erroneous conclusions and that explicit calculation of the cross section is necessary even for qualitative agreement with experiment. The method may still be useful, however, for a qualitative analysis of relative intensities of peaks pertaining to similar DOs.

It is also important to mention that the method presented here uses the dipole approximation, which is strictly valid only when the wavelength of the incident radiation can be considered to be large compared to molecular dimensions. In this region, the resulting photoelectron will have low kinetic energy. However, the PW and OPW approximations are valid only when the kinetic energy of the photoelectron is high. For photons with energy in the x-ray region, such as the ones generated by Mg $K\alpha$ radiation considered in this work (1253.6 eV), where the PW and OPW approximations are valid, the photon wavelength is already of molecular dimensions (9.9 Å), and the errors introduced by the dipole approximation are expected to be noticeable. For the treatment of larger molecules, or for more energetic photons, the use of the full form of the vector potential from Eq. (9) is expected to be important. This approach corresponds to allowance of all multipole moments (not only the dipole one). It was applied by Kaplan and Markin[23] in the x-ray photon range. In Ref. 47, it was developed for the γ-ray range where full relativistic calculation of the photoionization of H_2 up to photons with energy 1 MeV was performed.

A. CH_4

All the calculated relative photoionization intensities (Table II) reproduce the correct order. However, the PW results generally overestimate the intensities corresponding to the higher IPs. When the orthogonalization correction is applied, the results agree well with the experimental values. The DOs in CH_4 (Fig. 1) show a structure very similar to the canonical Hartree-Fock orbitals, and the diagonal approximations are already sufficient to reproduce the experimental data with high accuracy. Indeed, the highest intensity is noted for the first DO which is composed chiefly of the C 1*s* dominated $1a_1$ Hartree-Fock molecular orbital. The main contribution to the second DO, with intermediate intensity, comes from the C 2*s*-like $2a_1$ Hartree-Fock orbital. The least

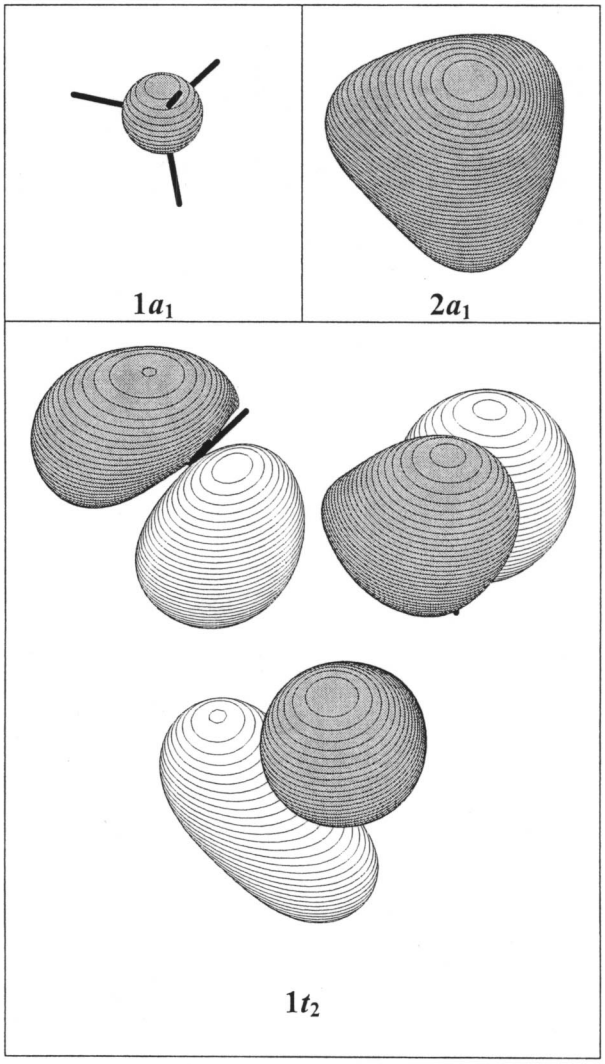

FIG. 1. Dyson orbitals for the CH_4 molecule.

intense feature comes from DOs that are dominated by the $1t_2$ Hartree-Fock orbitals which exhibit a mixing of C $2p$ and H $2s$ orbitals.

B. NH_3

The ammonia molecule poses a somewhat more interesting case. The correct intensity order is reproduced in all cases (Table III). Apart from the $1a_1$ ionization, which is underestimated, and the $2a_1$ in the P3 approximation, all intensities reproduce the experiment well. This last DO also has low pole strength, indicating that this state is not being described well by the P3 method. The intensities calculated from the canonical MOs are in close agreement with the experiment. The low pole strengths for the two higher ionization DOs in the diagonal approximations also indicate the possibility of shake-up lines, which are revealed by the nondiagonal calculations. The only important contribution to the $1a_1$ DO comes from the $1a_1$ Hartree-Fock orbital, which is dominated by N $1s$ basis functions. The DOs for NH_3 are depicted in Fig. 2.

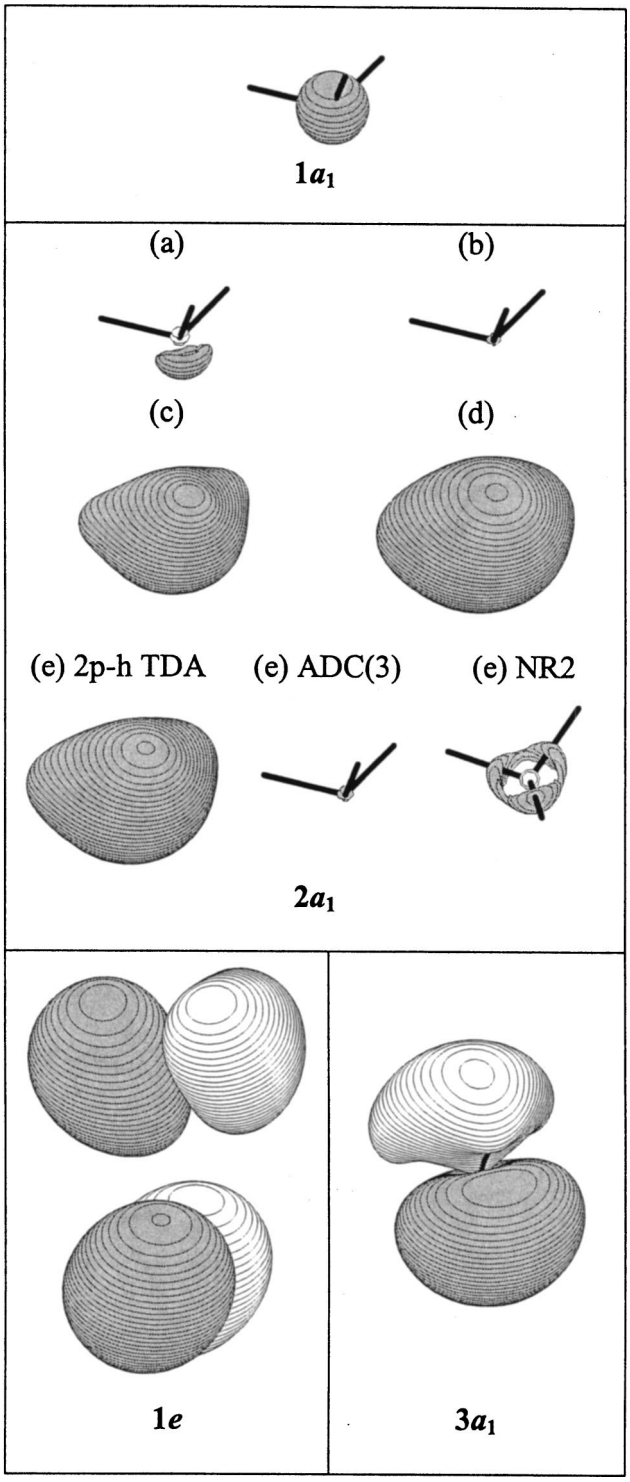

FIG. 2. Dyson orbitals for the NH_3 molecule.

The $2a_1$ ionization shows a structure of five lines in all nondiagonal methods. The structures of the DOs, in all cases, are combinations of the $2a_1$ and $3a_1$ Hartree-Fock orbitals, which can be identified with N $2s$ and N $2p_z$ basis functions, respectively, the dominant contributions being from the $2a_1$ orbital. The first four lines [$2a_1$ (a–d)] are similar in all approximations. The first line [$2a_1$-(a)] is the one with the highest contribution from $3a_1$ relative to $2a_1$. Comparison of the coefficients in the DO combination shows a $3a_1$ to

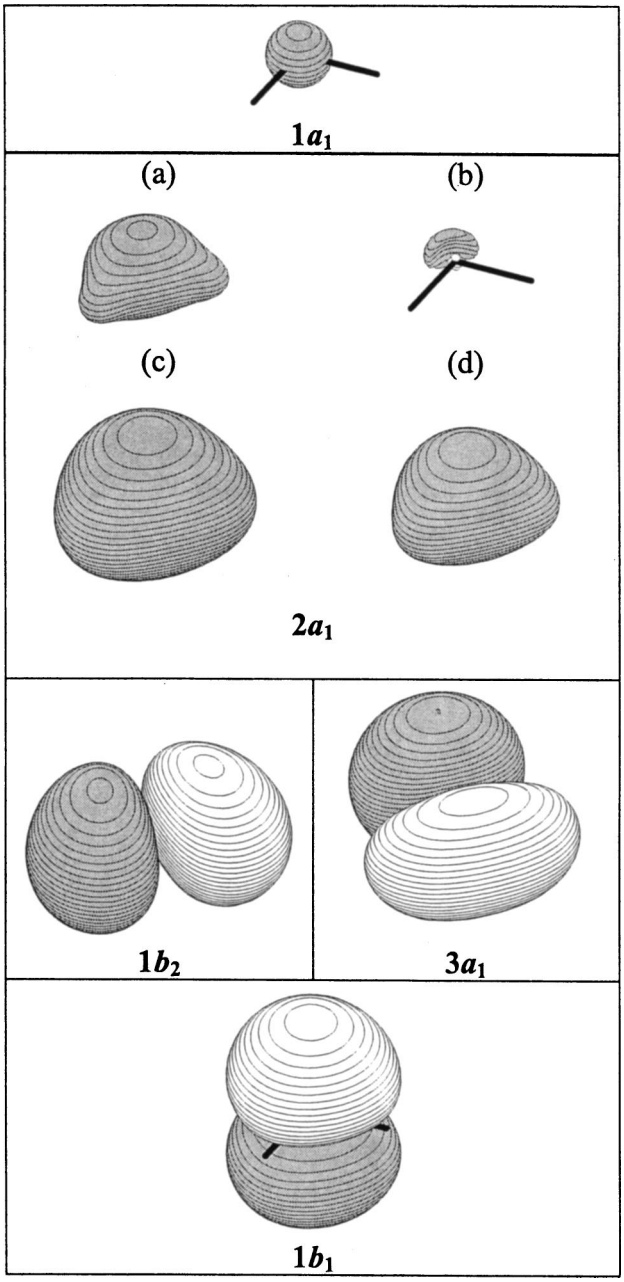

FIG. 3. Dyson orbitals for the H_2O molecule.

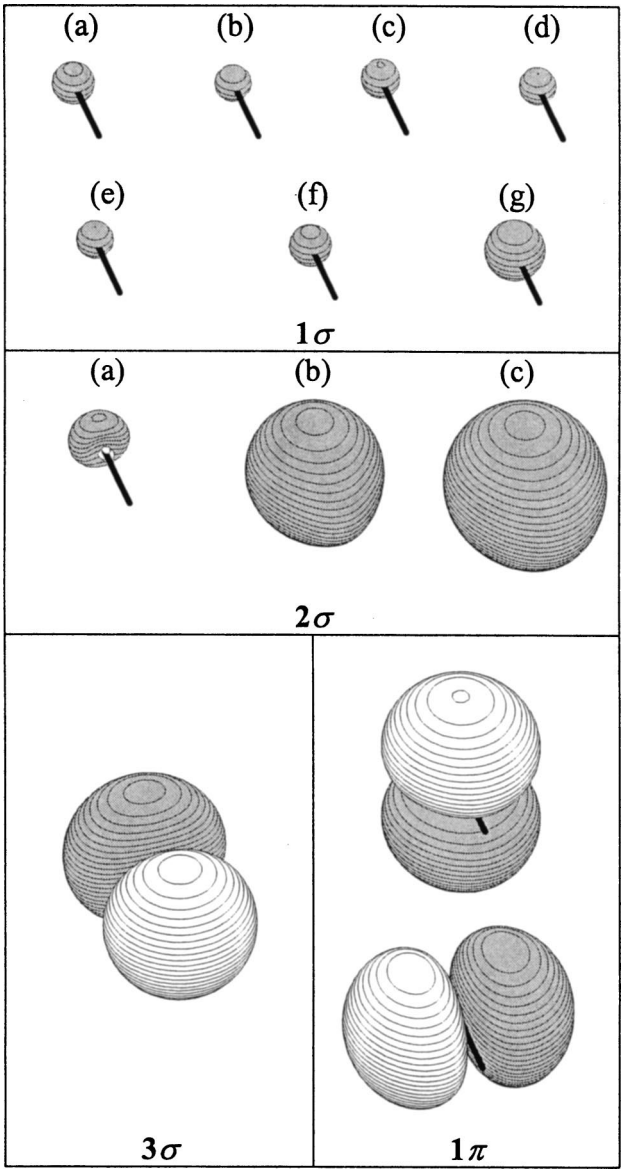

FIG. 4. Dyson orbitals for the HF molecule.

$2a_1$ ratio of 1:3. This high amount of $3a_1$ mixing is responsible for the lobe over the nitrogen atom seen in the plot. The $2a_1$-(b,d) poles have small contributions from both, but concentrate the DO more on the $2a_1$ HF orbital (1:14,1:9). The $2a_1$-(c) DO is composed almost exclusively of the $2a_1$ Hartree-Fock orbital (1:85). Also, the coefficient for the $2a_1$ orbital in the (c) and (d) cases is three to four times higher than in (a) and (b), which accounts for the size of the plotted contour. For the last [$2a_1$-(e)] DO, the $2ph$-TDA approximation concentrates most of the contributions in the $2a_1$ orbital, just like the $2a_1$-(c) DOs (1:87), while ADC(3) and NR2 both show more significant contributions from the $3a_1$ orbital, and reduced contributions from the $2a_1$, when compared to the $2ph$-TDA results. In the ADC(3) and NR2 cases the contribution from each HF orbital is small, like in the $2a_1$-(b) case, the ratio of $3a_1$ relative to $2a_1$ being 1:4 and 1:9, respectively, but the absolute contribution from the $2a_1$ orbital is higher in the NR2 case by ~36%.

Table VI shows the most important $2h$-p shake-up configurations that couple to the $2a_1$-h operator leading to a $^2A_1$ final state. The ionization of an inner-valence electron from the $2a_1$ DO is strongly mixed to processes which couple the

TABLE VI. Shake-up configurations for the NH_3 photoionization spectrum, from the NR2 calculation.

Final state		IP/eV (PS)	$\Sigma 2h$-p	Configurations
$^2A_1$	(a)	37.80 (0.02)	0.98	$0.28\,(1e)^{-1}(1e)^{-1}(na_1)^{+1}$
				$0.41\,(1e)^{-1}(1e)^{-1}(ne)^{+1}$
	(b)	34.62 (0.02)	0.98	$0.42\,(1e)^{-1}(1e)^{-1}(na_1)^{+1}$
				$0.38\,(1e)^{-1}(1e)^{-1}(ne)^{+1}$
	(c)	29.61 (0.21)	0.79	$0.53\,(1e)^{-1}(3a_1)^{-1}(ne)^{+1}$
				$0.14\,(3a_1)^{-1}(3a_1)^{-1}(na_1)^{+1}$
	(d)	27.05 (0.57)	0.43	$0.28\,(1e)^{-1}(3a_1)^{-1}(ne)^{+1}$
	(e)	26.37 (0.04)	0.96	$0.84\,(3a_1)^{-1}(3a_1)^{-1}(na_1)^{+1}$

TABLE VII. Shake-up configurations for the H_2O photoionization spectrum from the NR2 calculation.

Final state		IP/eV (PS)	$\Sigma 2h$-p	Configurations
$^2A_1$	(a)	37.45 (0.09)	0.91	$0.70\,(1b_2)^{-1}\,(3a_1)^{-1}\,(nb_2)^{+1}$
	(b)	33.78 (0.03)	0.97	$0.70\,(3a_1)^{-1}\,(3a_1)^{-1}(na_1)^{+1}$
				$0.13\,(1b_2)^{-1}\,(3a_1)^{-1}\,(nb_2)^{+1}$
	(c)	32.85 (0.63)	0.37	$0.13\,(1b_1)^{-1}\,(1b_1)^{-1}\,(na_1)^{+1}$
				$0.12\,(1b_2)^{-1}\,(3a_1)^{-1}\,(nb_2)^{+1}$
	(d)	30.30 (0.11)	0.89	$0.82\,(1b_1)^{-1}\,(1b_1)^{-1}\,(na_1)^{+1}$

ionization of a valence electron to the excitation of another valence electron. The cases where one $1e$ orbital is ionized while another is excited to an a_1 orbital or another e orbital generate the (a) and (b) states. Configurations with holes in the $1e$ and $3a_1$ orbitals and a particle in an e orbital are important in the (c) and (d) states. Finally, configurations where both excited and ionized electrons originate from the $3a_1$ HF orbital are the main component of the (e) state, but also contribute for the (c) state.

C. H_2O

All calculations reproduce the correct order of ionization intensities. The DOs for water are depicted in Fig. 3. As happened with the other examples, the approximations used here fail to reproduce quantitatively the intensities for the $1a_1\,(\mathrm{O}\,1s)$ ionizations, underestimating this intensity by around 40–50%.

The low pole strengths for the second-order and P3 poles for the $2a_1$ ionizations indicate a structure that is portrayed by the nondiagonal calculations as having four lines [$2a_1$ (a–d)]. Analysis of the DOs shows that the main component in all cases is the $2a_1$ Hartree-Fock orbital $(\mathrm{O}\,2s)$, with a small mixing of $3a_1\,(\mathrm{O}\,2s,2p_z,\mathrm{H}\,1s)$. The differences in intensities are due to differences in the $2a_1$ contribution for each DO, the main line [$2a_1$-(c)] being almost purely the $2a_1$ Hartree-Fock orbital. In the ADC(3) approximation, the roles of the $2a_1$-(b) and -(d) DOs are reversed. A higher contribution from the $2a_1$ Hartree-Fock orbital appears in the (b) rather than in the (d) component, as opposed to the $2ph$-TDA and NR2 cases. The sum of the calculated intensities from the four $2a_1$ lines agrees very well with the measured value. Also, the importance of the orthogonalization correction is evident from the results in Table IV.

Table VII shows the most important $2p$-h configurations coupling to the $2a_1$-h operator leading to a $^2A_1$ final state. The highest energy state (a) is mainly due to a configuration with holes in the $1b_2$ and $3a_1$ orbitals, and a particle in a b_2 orbital. This kind of configuration also contributes to the (b) state, which is dominated by a configuration where both holes are from the $3a_1$ orbital, with an excitation to an a_1 orbital. State (d) is dominated by a $1b_1$ ionization coupled to an excitation of a $1b_1$ electron to a $1a_1$ orbital. This last configuration is also partially responsible for the (c) state, together with another, where holes are left in both $1b_2$ and $3a_1$ orbitals and the particle in a b_2 orbital.

The $1b_2$ and $1b_1$ DOs do not show any mixing of Hartree-Fock orbitals and the results from the diagonal approximations are basically the same as in the nondiagonal approximations. The former DO displays a mix of $\mathrm{O}\,2p_y$ (in plane) and $\mathrm{H}\,1s$, while the latter consists almost entirely of $2p_x$ (out-of-plane) functions.

The main atomic contributions for the $3a_1$ DO come from $\mathrm{O}\,2s$ and $2p_z$ with some mixing with $\mathrm{H}\,1s$. This $\mathrm{O}\,2s$ contribution explains the high photoionization intensity when compared to the $1b_2$ and $1b_1$ lines. In the nondiagonal calculations, mixing from the $2a_1$ Hartree-Fock orbital increases the $\mathrm{O}\,2s$ character of the $3a_1$ DO and therefore increases the intensities relative to the diagonal results.

TABLE VIII. Shake-up configurations for the HF photoionization spectrum from the NR2 calculation.

Final state		IP/eV (PS)	$\Sigma 2h$-p	$2h$-p Configurations
$^2\Sigma(1\sigma)^b$	(a)	848.1(0.03)	0.97	$0.57\,(1\sigma)^{-1}\,(2\sigma)^{-1}\,(n\sigma)^{+1}$
				$0.29\,(1\sigma)^{-1}\,(1\pi)^{-1}\,(n\pi)^{+1}$
	(b)	838.6(0.01)	0.99	$0.13\,(1\sigma)^{-1}\,(2\sigma)^{-1}\,(n\sigma)^{+1}$
				$0.67\,(1\sigma)^{-1}\,(3\sigma)^{-1}\,(n\sigma)^{+1}$
				$0.12\,(1\sigma)^{-1}\,(1\pi)^{-1}\,(n\pi)^{+1}$
	(c)	827.8(0.02)	0.98	$0.25\,(1\sigma)^{-1}\,(3\sigma)^{-1}\,(n\sigma)^{+1}$
				$0.61\,(1\sigma)^{-1}\,(1\pi)^{-1}\,(n\pi)^{+1}$
	(d)	795.5(0.01)[a]	0.99	$0.61\,(1\sigma)^{-1}\,(2\sigma)^{-1}\,(n\sigma)^{+1}$
				$0.25\,(1\sigma)^{-1}\,(1\pi)^{-1}\,(n\pi)^{+1}$
	(e)	786.6(0.01)[a]	0.99	$0.80\,(1\sigma)^{-1}\,(2\sigma)^{-1}\,(n\sigma)^{+1}$
	(f)	774.7(0.03)	0.97	$0.27\,(1\sigma)^{-1}\,(2\sigma)^{-1}\,(n\sigma)^{+1}$
				$0.20\,(1\sigma)^{-1}\,(3\sigma)^{-1}\,(n\sigma)^{+1}$
				$0.39\,(1\sigma)^{-1}\,(1\pi)^{-1}\,(n\pi)^{+1}$
	(g)	695.6(0.83)	0.17	⋯
$^2\Sigma(2\sigma)^b$	(a)	43.45(0.02)	0.98	$0.83\,(3\sigma)^{-1}\,(3\sigma)^{-1}\,(n\sigma)^{+1}$
	(b)	40.97(0.36)	0.64	$0.56\,(1\pi)^{-1}\,(1\pi)^{-1}\,(n\sigma)^{+1}$
	(c)	38.20(0.53)	0.47	$0.32\,(1\pi)^{-1}\,(1\pi)^{-1}\,(n\sigma)^{+1}$

[a]From $2p$-h TDA calculation.
[b]Indicates the dominant HF orbital contribution in the Dyson orbitals combinations.

D. HF

Relative intensity results for the HF molecule are shown in Table VII and the DOs are depicted in Fig. 4. Diagonal approximations completely fail to reproduce the experiment in the inner valence and core regions. The results show that these ionizations are accompanied by a number of shake-up processes. Nondiagonal approximations are necessary for an appropriate description of the photoelectron spectrum of this molecule. The 1σ DOs correspond to a main peak [1σ (g)] and seven secondary peaks [1σ (a–f)] in the $2p$-h TDA approximation. Four of those lines (a,b,c,f) appear in the NR2 approximation, while ADC(3) locates only three of them (a,b,f). The most important contribution to the DO, in all cases, comes from the 1σ Hartree-Fock $(\mathrm{F}\,1s)$ orbital. The shake-up configurations in Table VIII show that those states are generated by the coupling of an ionization with an excitation, where one hole is always on the 1σ orbital and the other in any of the inner-valence or valence orbitals.

The 2σ DOs correspond to two states with comparable intensities [2σ (b,c)] and a third weak feature at a slightly higher energy, labeled 2σ (a). The DOs for all three peaks are composed primarily of the 2σ (mostly $\mathrm{F}\,2s$) Hartree-Fock orbital with a small mixing from the 3σ (mostly $\mathrm{F}\,2p_z$).

Table VIII shows that both stronger lines have very similar structures with significant coupling from a shake-up configuration where one π electron is ionized while another is excited to a σ orbital, while for the higher energy feature both ionization and excitation to a σ orbital originate from the 3σ. The relative contribution of the 2σ orbital is five to eight-times larger in the (b) and (c) peaks when compared to the (a) peak, which explains the difference in intensities and in the size of the contour plot (Fig. 4). Neither the PW nor OPW approximation agrees quantitatively with the experimental intensity, but the importance of the orthogonalization correction is evident. The experimental reports do not discuss such features. However, the spectrum from Ref. 44 shows an asymmetric peak, centered at 39.65 eV, slightly broader to the low energy side, obtained by fitting a Lorentzian function to the peak in the experimental spectrum. Our results suggest that the use of at least two fitting functions could be appropriate.

The last two ionization lines are well described by the diagonal approximations as shown by the high pole strengths, and the relative intensities are in reasonable agreement with the experimental values.

VI. CONCLUSIONS

A program was implemented in the GAUSSIAN package to perform *ab initio* electron propagator calculations of photoelectron intensities in the dipole approximation, applying either a plane-wave or orthogonalized plane-wave description of the photoelectron. Applications to the first-row hydrides satisfactorily predict the photoelectron spectra for all molecules. The correct order of ionization intensities is reproduced in all cases and, with the exception of core ionizations, a semiquantitative agreement is possible when the orthogonalized plane wave is used.

Shake-up states in NH_3, H_2O, and HF were located and their intensities relative to those of the primary (h,p) part of each spectrum were calculated. Important $2p$-h configurations in these states were discussed. Calculations of the intensity pertaining to shake-up states proved crucial for the correct interpretation of the NH_3 and H_2O inner-valence spectra. The existence of shake-up states not previously reported for HF suggests that a reevaluation of the experimental data might be appropriate.

Nondiagonal approximations are advantageous for cases when several final states corresponding to the same irreducible representation symmetry are present, as in H_2O. These methods also are useful for examination of inner-valence IEs with similar DOs. None of these approximations, however, provided consistently better results and therefore a choice of method may be based on computational efficiency alone. The NR2 method is the most easily executed of the nondiagonal approximations. For simpler systems where a single-determinant description of the final state is suitable, such as CH_4, the diagonal approximations can be used. In this case, the P3 method is indicated.

With appropriate choices of the photoelectron representation, the EPT approximation, and the basis set, the methods described here can be a useful tool for the interpretation of photoelectron spectra.

ACKNOWLEDGMENTS

The authors would like to thank the National Science Foundation Grant No. CHE-0125823, the American Chemical Society—Petroleum Research Fund Grant No. 34859-AC6, and Kansas DEPSCoR.

[1] K. Siegbahn, C. Nordling, G. Johansson *et al.*, *ESCA Applied to Free Molecules* (Elsevier, New York, 1969).
[2] D. W. Turner, C. Baker, A. D. Baker, and C. R. Brundle, *Molecular Photoelectron Spectroscopy—A Handbook of He 584 Å Spectra* (Wiley-Interscience, London, 1970).
[3] J. K. P. Metzker, N. E. Gruhn, and D. L. Litchenberger, J. Phys. Chem. A **106**, 9999 (2002).
[4] T. Koopmans, Physica (Amsterdam) **1**, 104 (1933).
[5] A. Szabo and N. S. Ostlund, *Modern Quantum Chemistry. Introduction to Advanced Electronic Structure Theory* (Dover, New York, 1996).
[6] O. Goscinski and B. Lukman, Chem. Phys. Lett. **7**, 573 (1970).
[7] Y. Öhrn and G. Born, Adv. Quantum Chem. **13**, 1 (1981).
[8] J. Schirmer, L. S. Cederbaum, and O. Walter, Phys. Rev. A **28**, 1237 (1983).
[9] W. von Niessen, J. Schirmer, and L. S. Cederbaum, Comput. Phys. Rep. **1**, 57 (1984).
[10] V. G. Zakrzewski, J. V. Ortiz, J. A. Nichols, D. Heryadi, and D. L. Yeager, Int. J. Quantum Chem. **60**, 29 (1996).
[11] J. V. Ortiz, J. Chem. Phys. **104**, 7599 (1996).
[12] J. V. Ortiz, in *Computational Chemistry—Review of Current Trends*, edited by J. Leszczynski (World Scientific, Singapore, 1997), Vol. 2, p. 1.
[13] J. V. Ortiz, V. G. Zakrzewski, and O. Dolgounitcheva, in *Conceptual Perspectives in Quantum Chemistry*, edited by J.-L. Calais and E. Kryachko (Kluwer, Dordrecht, 1997), Vol 3, p. 465.
[14] J. V. Ortiz, J. Chem. Phys. **108**, 1008 (1998).
[15] A. M. Ferreira, G. M. Seabra, O. Dolgounitcheva, V. G. Zakrzewski, and J. V. Ortiz, in *Quantum Mechanical Prediction of Thermochamical Data*, edited by Cioslowski (Kluwer, Dordrecht, 2001), p. 131.
[16] O. Dolgounitcheva, V. G. Zakrzewski, and J. V. Ortiz, J. Phys. Chem. A **106**, 8411 (2002).
[17] O. Dolgounitcheva, V. G. Zakrzewski, and J. V. Ortiz, Int. J. Quantum Chem. **65**, 463 (1997).
[18] O. Dolgounitcheva, V. G. Zakrzewski, and J. V. Ortiz, Int. J. Quantum Chem. **90**, 1547 (2002).
[19] O. Dolgounitcheva, V. G. Zakrzewski, and J. V. Ortiz, in *Fundamental World of Quantum Chemistry: A Tribute to Per-Olov Löwdin*, edited by E. J. Brändas and E. S. Kriachko (Kluwer, Dordrecht, 2003), Vol. 2, p. 525.
[20] M. J. Frisch, G. W. Trucks, H. B. Schlegel *et al.*, GAUSSIAN 03, Revision B.0, Gaussian, Inc., Pittsburgh, PA, 2003.
[21] H. A. Bethe and E. E. Salpeter, *Quantum Mechanics of One- and Two-Electron Atoms* (Springer, Berlin, 1957).
[22] I. G. Kaplan and A. P. Markin, Opt. Spektrosk. **24**, 884 (1968); **25**, 493 (1968).
[23] I. G. Kaplan and A. P. Markin, Doklady Akademii Nauk SSSR **184**, 66 (1969).
[24] L. L. Lohr and M. B. Robins, J. Am. Chem. Soc. **92**, 7241 (1970).
[25] L. L. Lohr, Jr., *Electron Spectroscopy: Proceedings of an International Conference held at Asilomar, Pacific Grove, California, USA, 7–10 September, 1971*, edited by D. A. Shirley (Elsevier, New York, 1972), p. 245.
[26] W. Thiel and A. Schweig, Chem. Phys. Lett. **12**, 49 (1971); **21**, 541 (1973).
[27] F. O. Ellison, J. Chem. Phys. **61**, 507 (1974).
[28] J. W. Rabalais, T. P. Debies, J. L. Berkowsky, J.-T. J. Huang, and F. O. Ellison, J. Chem. Phys. **61**, 516 (1974).
[29] B. Pickup, Chem. Phys. **19**, 193 (1977).
[30] G. D. Purvis and Y. Öhrn, J. Chem. Phys. **62**, 2045 (1975).
[31] G. Born and Y. Öhrn, Phys. Scr. **21**, 378 (1980).
[32] M. Mishra and Y. Öhrn, Int. J. Quantum Chem. **S14**, 335 (1980).
[33] M. Deleuze, B. T. Pickup, and J. Delhalle, Mol. Phys. **83**, 655 (1994).
[34] M. Deleuze and L. S. Cederbaum, Int. J. Quantum Chem. **63**, 465 (1997).
[35] G. C. Schatz and M. A. Ratner, *Quantum Mechanics in Chemistry* (Prentice Hall, London, 1993), p. 57.

[36] E. Merzbacher, *Quantum Mechanics* (Wiley, New York, 1961), p. 439.
[37] S. F. Boys, Proc. R. Soc. London, Ser. A **200**, 542 (1950).
[38] P. Kaijser and V. D. Smith, Jr., Adv. Quantum Chem. **10**, 37 (1977).
[39] H. W. Press, S. A. Teukolsky, W. T. Vetterling, and B. P. Flannery, *Numerical Recipes in Fortran 77—The Art of Scientific Computing*, 2nd edn. (Cambridge University Press, Cambridge, 1986), p. 191.
[40] A. R. Curtis and C. W. Clenshaw, Numerische Matematik **2**, 197 (1960).
[41] T. H. Dunning, Jr., J. Chem. Phys. **90**, 1007 (1989).
[42] G. Schaftenaar and J. H. Noordik, J. Comput.-Aided Mol. Des. **14**, 123 (2000).
[43] D. A. Allison and R. C. Cavell, J. Chem. Phys. **68**, 593 (1978).
[44] M. S. Banna, B. E. Mills, D. W. Davis, and D. A. Shirley, J. Chem. Phys. **61**, 4780 (1974).
[45] M. S. Banna and D. A. Shirley, J. Chem. Phys. **63**, 4759 (1975).
[46] C. S. Fadley, Chem. Phys. Lett. **25**, 225 (1974).
[47] I. G. Kaplan and A. P. Markin, Zh. Eksp. Teor. Fiz **64**, 424 (1973).